Photoinduced Transformations in *Bacteriorhodopsin* Membrane Monitored with Optical Microcavities

Juraj Topolancik and Frank Vollmer *

Rowland Institute at Harvard, Harvard University, Cambridge, MA 02142

ABSTRACT Photoinduced molecular transformations in a self-assembled *Bacteriorhodpsin* (*bR*) monolayer are monitored by observing shifts in the near-IR resonant wavelengths of linearly polarized modes circulating in a microsphere cavity. We quantify the molecular polarizability change upon all-*trans* to 13-*cis* isomerization and deprotonation of the chromophore retinal (~-57Å^3) and determine its orientation relative to the *bR* membrane (~61°). Our observations establish optical microcavities as a sensitive off-resonant spectroscopic tool for probing conformations and orientations of molecular self-assemblies and for measuring changes of molecular polarizability at optical frequencies. We provide a general estimate of the sensitivity of the technique and discuss possible applications.

---

* e-mail: vollmer@rowland.harvard.edu

INTRODUCTION

Optical microresonators with small modal volumes and high quality (Q) factors significantly enhance interaction of the optical field with the material through recirculation, which makes them exceptionally sensitive to the optical properties of the resonator (1-3) and the surrounding medium (4-8). Exploiting this attribute, optical microcavities have been used successfully for ultra-sensitive detection of heavy water (5) and biomolecules (6-8). In biosensing, the sensitivity of microcavities rivals that of surface-plasmon resonance (SPR) (9) and waveguide-based spectroscopy (10,11) which are recognized as state-of-the-art label-free detection techniques. Binding of only a few molecules on the microcavity surface shifts the frequencies of the resonant modes that evanescently interact with the adsorbed material. Monitoring of the shift induced by changes of the molecular polarizability forms the basis of label-free, non-invasive, real-time biodetection (6,7) and nanolayer characterization (8). It would be intriguing to further extend this sensitive technique to study optical anisotropies and to track dynamic changes in molecular structure. In this context, proteolipid membranes are a particularly relevant subject for investigations as they are central to many areas of life sciences and are difficult to study with traditional optical techniques, with notable exceptions of optical-waveguide lightmode spectroscopy (OWLS) (11) and coupled plasmon-waveguide resonance (CPWR) (12). These optical-waveguide-based techniques utilize two orthogonal polarizations of evanescent optical fields, transverse magnetic (TM) and transverse electric (TE). This allows them to probe optical anisotropies (12,13) and to monitor conformational changes in biological membranes immobilized onto solid waveguide surfaces (14).

High-Q optical microcavities represent an interesting alternative to the waveguide-based techniques providing exceptional sensitivity (6-8), straightforward in-plane optical integration on micron scales and, as we will show, two probing polarizations and operation at arbitrary wavelengths. The possibility to use two orthogonally polarized resonant modes in microresonators for biosensing has not yet been explored. This report extends the detection capabilities of microcavities by allowing anisotropy measurements. The operation at arbitrary wavelengths is particularly important for non-invasive sensing because an optical probe could trigger molecular transitions in binding macromolecules, which would interfere with the analysis. This is the case for example with photosynthetic pigments (15) or *Rhodopsins* (16) that contain light-absorbing chromophores in the membrane. We find that anisotropies of such systems can be probed with high-Q microresonators using polarized modes at wavelengths far from any molecular absorption, e.g. in the near-infrared (near-IR). Furthermore, a pump-probe spectroscopy can be implemented where an optical pump centered at the molecular resonance induces structural changes which are then dynamically monitored off-resonance with a probe. In this article, we demonstrate this approach by measuring molecular structural changes in the biological photochrome *bacteriorhodopsin (bR)*. *bR* is ideal for such a demonstration since its structure is well known (16-18), it self-assembles easily onto a silica surface (19,20) and its molecular conformation can be switched optically between two stable states (21). We study the photochromic transitions of the chromophore retinal in *bR* by monitoring the shift of polarized whispering-gallery modes (WGMs) in the near-IR. We quantitatively analyze the associated molecular polarizability changes and show that the shift ratio for the two polarizations reflects the orientation of the retinal with respect to the resonator surface. We further discuss limitations and possible applications of the introduced spectroscopic technique.

EXPERIMENTAL PROTOCOL

Experimental setup

The optical setup used in our experiments in shown schematically in Fig. 1(a). A sample cell was constructed by threading a single mode optical fiber (SMF-28) through a 1 cm polystyrene cuvette. The fiber with a stripped polymer sheath was glued to the sides of the container and the exposed silica was etched with a 50% hydrofluoric (HF) acid solution. After a ~30-minute etch a taper with a diameter of ~2-3 μm was formed, as observed with an upright microscope equipped with a long working distance objective. The taper was used to excite WGMs in optical resonators by evanescent field coupling. A silica microsphere (~300 μm diameter) on-a-stem was prepared by melting the tip of a SMF-28 fiber in a butane-N_2O flame. It was then mounted on a mechanical stage and brought in contact with the taper as shown in Fig. 1(b). A tunable distributed-feedback (DFB) laser diode (probe) operating around $\lambda_{probe}\cong 1{,}310$ nm was coupled into the taper and a photodiode (PD_1) at the other end of the fiber recorded the transmission. WGMs were identified as Lorentzian-shaped troughs in a spectrum obtained by periodically tuning the DFB laser current (I) at 100 Hz with a waveform generator. The laser tuning coefficient $\Delta\lambda/\Delta I$ ~0.0055 nm/mA was determined with a wavemeter. Spectra containing 1,000 points per scan were recorded every ~200 ms and the positions of the resonances were tracked with a computer using a LABVIEW routine based on polynomial fitting algorithm. The width (at half-maximum) of these troughs reflects the intrinsic Q-factor and absorbance of the material surrounding the cavity. A polarizer (P_1) and a rotating half-waveplate were used to selectively excite either TE or TM resonances. The polarization direction of the monitored mode was verified by analyzing the light scattered tangentially off the microsphere, using another polarizer (P_2) and a photodiode (PD_2),. This arrangement was used to optimize the mode coupling efficiency into the resonator by slowly etching the microsphere and the fiber with a highly diluted HF solution (<1%). The process was terminated when the probe was critically coupled into the cavity, i.e. when almost no light was transmitted on resonance, at which point the sample cell was rinsed and filled with a 10 mM phosphate buffered saline (PBS) solution (pH=7.4) Another semiconductor laser (pump) emitting at $\lambda_{pump}\cong 532$ nm was coupled into the same tapered fiber. This green pump was used to trigger photoinduced structural changes in *bR* which was later adsorbed onto the surface of the silica microsphere.

Bacteriorhodopsin adsorption

bR forms a 5nm-thick membrane with a well defined surface density of monomers (17). Each momoner contains a retinal chromophore surrounded by a seven-α-helix trans-membrane protein which is embedded in a lipid bilayer composed of ten *Haloarchaeal* lipids per *bR* monomer (Fig. 1 (c)). The retinal is covalently bound to Lys216 residue via a protonated Schiff base (SB) at a fixed angle relative to the proteolipid membrane. *bR* thin-film formation on solid surfaces has been widely studied in the context of fabrication of optoelectronic devices and various techniques for controlled immobilization of oriented monolayers have been demonstrated (19,20). In our study we used the electrostatic deposition of *bR* onto a PDAC-coated silica microsphere (20), which was optimized for a monolayer formation. The microsphere was sonicated for 15 minutes in 350 mM solution of KOH after which a positively charged polymer poly(dimethyldiallyl)ammoniumchloride (PDAC) was pre-adsorbed onto its surface to promote successive binding of the negatively charged *bR* membranes. This was done by exposing the sphere to a 2% PDAC solution in 0.5 M NaCl at a pH of 6.8 for 2 minutes. The sphere was then rinsed in distilled water for additional 2 min. The *bR* layer was formed *in situ* using 1 mg/ml sonicated stock solution of D96N *bR* mutant (Munich Innovative Biosystems) in Milli-Q water which was further diluted (molar ratio 1:10) upon injection into the sample cell filled with PBS.

RESULTS

Monolayer formation

The *bR* adsorption process was monitored by tracking the resonant wavelength shift of a TM mode (6). The time-trace of the shift shows Langmuir-like adsorption kinetics which points to self-assembly of a single layer at saturation (Fig. 2). The absorption trace can be fit well by: $\Delta\lambda = \Delta\lambda_{sat}\left(1 - e^{-t/\tau}\right)$, where $\Delta\lambda_{sat} \cong 67$ pm is the wavelength shift at saturation and $\tau \approx 33$ min. Adsorption of the ultra-thin oriented *bR* layer does not significantly degrade the cavity Q which remains in the 10^6 range. The monolayer formation is further confirmed by estimating the surface density of *bR* monomers, σ_{bR}, in the adsorbed layer which can be extracted from the resonant shift (22):

$$\sigma_{bR} \approx \left(\frac{\Delta\lambda}{\lambda}\right)\frac{\varepsilon_0\left(n_s^2 - n_m^2\right)R}{\alpha_{bR}}, \tag{1}$$

where $\Delta\lambda/\lambda$ is the fractional resonant wavelength shift at saturation, R is the microsphere radius, α_{bR} is the molecular polarizability in excess to that of the displaced water, and n_s and n_m are the refractive indices of the sphere (1.47) and the PBS solution (1.33), respectively. The total excess polarizability of one *bR* monomer for a TM mode α_{bR} is the sum of the protein (α_P), the lipids (α_L), and the retinal (α_R) contributions: $\alpha_{bR} = \alpha_P + \alpha_L + \alpha_R = 1.05\times10^4$ au + 5.73×10^3 au + 160 au $\approx 1.64\times10^4$ au (~2.4×10^3 Å^3) (23-25). Summing up the individual contributions we can use Eq. 1 to evaluate σ_{bR}. The obtained value of 9.8×10^{12} cm^{-2} is somewhat higher than the reported *bR* surface density in a monolayer (9.12×10^{12} cm^{-2}) determined from X-ray scattering measurements (17). This indicates that our self-assembly procedure yields a high surface coverage with slightly overlapping *bR* fragments, in agreement with observations reported in literature (20).

Molecular structural changes

Illumination of *bR* around 568 nm triggers a complex photocycle that contains spectroscopically distinct intermediaries J, K, L, M, N, and O. The photoexcitation process involves isomerization and a slight rotation of the chromophore retinal, a proton transfer across the lipid membrane (16), and significant protein conformational changes (26). Throughout the photocycle, the chromophore retinal changes its conformation between the all-*trans,* 15-*anti* protonated SB found in the thermodynamically stable ground state; and the 13-*cis,* 15-*anti* deprotonated SB prevalent in the metastable M state. The *bR* absorption peak shifts from 568 nm to 412 nm in the process of the ground to the M-state transformation. In the absence of the photoexcitation, M state relaxes spontaneously into the thermodynamically stable ground state through N and O intermediaries. The use of D96N mutant (27) with an extended M state lifetime ensures complete *bR* conversion.

The spectral shift of the *bR* absorption maxima due to the photochemical transformation has been shown to cause significant refractive index changes (Δn) of *bR* films. This is especially the case with D96N in which Δn is about four times larger than in the wild type *bR* (28). Wavelength-dependent measurements of the index changes $\Delta n(\lambda)$ performed on *bR* films show a distinct maximum near the ground state absorption band at a slightly longer wavelength, and the index change is progressively smaller at longer wavelengths where *bR* is increasingly transparent (28). More specifically, the maximum index change recorded around 633 nm is $\Delta n \cong -4\times10^{-3}$ while at 800 nm it is only $\Delta n \cong -1\times10^{-3}$ (28). The large measured index change at 633 nm has been exploited for all-optical modulation in a novel integrable component based on OWLS technique (29), but, to our knowledge, the possibility to probe *bR* far from its electronic transitions has not been explored.

In our measurements the state of the *bR* is controlled with a low power (<200 μW), continuous wave, green pump laser coupled to the microsphere cavity using the tapered fiber (Fig. 1(a)). The visible pump evanescently excites WGMs propagating around the microsphere's equator inducing the ground to the M state conversion along their path. At the same time, a near-IR beam ($\lambda_{probe} \cong 1{,}310$ nm) excites the probing resonances. The approximate bulk index change upon isomerization at the probing wavelength is only $\sim -8\times10^{-4}$, as extrapolated from the Kramers-Kronig transformation of the published absorption data (28). The photoexcitation of the retinal reduces the refractive index of *bR* which causes a negative shift of the TE and TM resonances (Fig. 3). *bR* forms an anisotropic, ultra-thin macromolecular monolayer on the cavity surface where the evanescent field intensity is the highest. Although only a small fraction of the evanescent tail interacts with the *bR* membranes, we are sensitively probing molecular changes in a highly oriented anisotropic system. We therefore choose polarizability rather than refractive index to describe the photochromic transitions. Given the measured surface density of *bR* monomers, Eq. 1 can be used to calculate the average polarizability change at λ_{probe} of a single *bR* molecule upon photoexcitation: $\langle \Delta\alpha_{avg} \rangle = \frac{1}{3}\left(\langle \Delta\alpha_{TM} \rangle + 2\langle \Delta\alpha_{TE} \rangle\right) = -384$ au (~ -57 Å^3). The value reflects structural changes of the retinal in its complex proteolipid environment. On the molecular level, the measured shifts of resonances are caused by the change of the retinal polarizability tensor and the related conformational changes in the surrounding protein. Our experiments show that off-resonant monitoring of structural changes and anisotropies in optically active materials is possible with high-Q optical microcavities, even when the changes occur in optically dilute molecular monolayers.

To test the validity of the introduced method, we compare the polarizability change $\left\langle \Delta\alpha_{avg}(1310nm) \right\rangle$ to the corresponding polarizability and index changes measured in *bR* thin-films with the established optical techniques (28, 29). Since Δn depends on the optical density (OD) and pH of the *bR* film, we use published results obtained on a film with a moderate OD of 3.6 and pH of 8 in which the maximum measured refractive index change was Δn(633nm)≅-4×10^{-3} (28). The Lorenz-Lorentz formula was applied to express the refractive index change as the change of the molar refraction $\Delta R = R_M - R_{ground}$=$-3.6\times10^{-22}$ cm^3 $molecule^{-1}$. Using the standard definition of molar refraction: $R(\lambda) = \frac{4\pi}{3} N_A \alpha(\lambda)$, where N_A in the Avogadro's constant, we obtain the corresponding change of the molecular polarizability of a single *bR* monomer $\Delta\alpha$ (633nm)≅-580 au (-86 $Å^3$). Since the probing wavelength is within the absorption band of the ground state, the result is an approximate lower limit of the polarizability change. As expected, the absolute value is larger than the one we measured with WGMs far from the absorption band at 1,310nm.

Time response study

Time-resolved switching data for a step modulation of a low-intensity, continuous wave pump is presented in Fig. 3. Since the intensity of the pump is resonantly enhanced by recirculation in the microcavity, moderate pump powers (<200 μW) are sufficient to fully photoexcite *bR* molecules. The time traces of near-IR resonant wavelength positions for two polarizations reveal a fast timescale associated with the photoinduced M state buildup and a slow thermal relaxation into the ground state at τ~11s. The results are consistent with the timescales of photochromic transformations of D96N. In the absence of pulsed excitation and triggered, high-speed data acquisition, faster transition timescales corresponding to the transient intermediaries J, K, L, N and O were not resolved in our measurements. In principle, microcavities can monitor molecular processes in real time if their timescales are longer than the cavity photon lifetime, $\tau_{cav} = \frac{Q}{2\pi\nu}$, where Q is the cavity quality factor, and ν is the frequency of the probing light. With Q~10^6 and ν~2×10^{14} Hz, silica microspheres should be able to dynamically resolve nanosecond transitions and quantify molecular polarizabilities of the corresponding intermediaries.

Retinal orientation

We have consistently observed the shift ratio for the TE and TM polarizations ($\Delta\lambda_{TE}/\Delta\lambda_{TM}$) of 2.1±0.1 (Fig. 4). This, as we are going to show, can be directly related to the orientation of the retinal relative to the *bR* membrane. We define the orientation angle θ as the angle between the membrane normal and the C_5-C_{13} bond in the retinal (inset of Fig. 4). Retinal isomerization changes the dipole moment induced by the evanescent field of the optical resonance. This causes a change of the photon energy of the resonant state, which shifts the resonant frequency ω by:

$$\hbar\delta\omega \approx -\frac{1}{2}\vec{E}(\vec{r},t)\cdot\delta\hat{\alpha}\cdot\vec{E}^*(\vec{r},t)\,, \tag{2}$$

where $\vec{E}(\vec{r},t)$ is the electric-field vector of the probing mode and $\delta\hat{\alpha}$ is the tensor describing the polarizability change. In our analysis we consider the retinal as rod-like molecule undergoing changes of the molecular polarizability $\delta\alpha_{//}$ and $\delta\alpha_{\perp}$ along the major retinal axis ($\hat{e}_{//}$) and perpendicular to it ($\hat{e}_{\perp}$), respectively. We ignore the slight rotation of the retinal polarizability axis caused by the structural transformation (18), and consider the molecule to be oriented at a fixed average angle $\langle\theta\rangle$ from the membrane plane normal (z) (Fig. 5). We use the longitudinal $\langle\theta\rangle$ and the azimuthal angle ϕ to define the orientation of the retinal with respect to the polarization directions of the resonant modes oriented along the x- (TE) and z-axis (TM). For the TM mode, $\langle\theta\rangle$ is constant for all possible in-plane orientations of the retinal. The fractional wavelength shift for TM modes upon retinal isomerization can be expressed in terms of $\langle\theta\rangle$ and the changes of molecular polarizabilities $\delta\alpha_{//}$ and $\delta\alpha_{\perp}$ as:

$$\frac{\Delta\lambda_{TM}}{\lambda} \approx \left(\delta\alpha_{\perp}\sin^2\langle\theta\rangle + \delta\alpha_{//}\cos^2\langle\theta\rangle\right)\frac{|E_{TM}|^2}{2E_0}\,. \tag{3}$$

Here $|E_{TM}|^2$ is the average field amplitude of the TM mode at the resonator surface and $E_0 = \int \varepsilon_s |\vec{E}(\vec{r})|^2\,dV$ is the total electromagnetic mode energy contained in the interior of the microsphere with permittivity ε_s.

For the TE polarization the angle between the polarization direction (x) and the molecular axis varies with the retinal in-plane orientation represented by the azimuthal angle ϕ. Averaging this over all possible angles ϕ to account for contributions of retinals randomly oriented in the membrane plane we obtain:

$$\frac{\Delta\lambda_{TE}}{\lambda} \approx \frac{1}{2}\left[\delta\alpha_{\perp}(1+\cos^2\langle\theta\rangle) + \delta\alpha_{//}\sin^2\langle\theta\rangle\right]\frac{|E_{TE}|^2}{2E_0}\,. \tag{4}$$

The ratio of the resonant shifts for the TE and TM polarizations then becomes:

$$\frac{\Delta\lambda_{TE}}{\Delta\lambda_{TM}} \approx \frac{1}{2}\left[\frac{\delta\alpha_{\perp}(1+\cos^2\langle\theta\rangle) + \delta\alpha_{//}\sin^2\langle\theta\rangle}{\delta\alpha_{\perp}\sin^2\langle\theta\rangle + \delta\alpha_{//}\cos^2\langle\theta\rangle}\right]\frac{|E_{TE}|^2}{|E_{TM}|^2}\,. \tag{5}$$

To simplify this equation further we assume equal amplitudes of TE and TM whispering gallery modes, i.e. $|E_{TE}|^2 \approx |E_{TM}|^2$; as confirmed (within ~±10% variation) by measurements of wavelength shifts due to absorption of globular proteins (25). $\langle\theta\rangle$ is related to the wavelength shift ratio of TE and TM modes upon retinal isomerization by:

$$\frac{\Delta\lambda_{TE}}{\Delta\lambda_{TM}} \approx \frac{1}{2}\left(\frac{1+\cos^2\langle\theta\rangle+\beta\sin^2\langle\theta\rangle}{\sin^2\langle\theta\rangle+\beta\cos^2\langle\theta\rangle}\right). \tag{6}$$

Here β denotes the ratio of the photoinduced changes in α along and perpendicular to the major molecular axis which we define here along the C_5-C_{13} bond; $\beta = \delta\alpha_{//}/\delta\alpha_{\perp}$. According to results of *ab initio* calculations of α (24), $|\delta\alpha_{//}|$ is an order of magnitude lager than $|\delta\alpha_{\perp}|$, and therefore $\beta \approx -10$. The value is negative because the *trans*-*cis* isomerization of C_{13}-C_{14} bond causes the polarizability to decrease along the major molecular axis and increase perpendicular to it. As it is difficult to numerically study the full *bR* membrane structure with all of its proteolipid components only the chromophore retinal has been considered in these tentative calculations. The results for the retinal orientation are relatively insensitive to the precision of β values used in the calculation. The measured value of $\Delta\lambda_{TE}/\Delta\lambda_{TM}$ corresponds to $\langle\theta\rangle$ of ~61°. It is interesting to compare this result to measured retinal orientations obtained with alternative methods. The value is in excellent agreement with the reported average angle obtained with 3D X-ray diffraction; $\langle\theta\rangle \cong 60.7°$ (18). It is however considerably smaller than the orientation angle of the optical transition dipole that has been measured at 69.0° in the ground and at 66.9° in the M state, i.e. $\langle\theta\rangle \cong 68°$ (33). Our experiments in the present form do not provide direct means to determine orientation of the transition dipole. The dipole axis is not aligned with the C_5-C_{13} bond, but its orientation can be investigated experimentally with microspheres by controlling the polarization direction of the pump. Different excitation efficiencies for TE- and TM-polarizations would reveal the orientation of the optical transition dipole. It should be noted that, since we assumed axial symmetry of the retinal and disregarded the slight change of θ upon photoexcitation in the derivation of Eq. 6, and used an approximate computed value of β to get $\langle\theta\rangle$, the excellent agreement with the high-resolution structural data might be somewhat fortuitous. Nevertheless, our experiments indicate that orthogonally polarized resonant modes in silica microspheres can non-invasively probe optical anisotropies in molecular monolayers. Finally, we also want to emphasize that the technique described herein cannot distinguish between the two possible binding *bR* membrane orientations, i.e. they cannot determine the respective fractions of *bR* fragments bound to the surface with its cytoplasmic and extracellular side. This however has no bearing on the conclusions regarding the polarizability values and the retinal orientations.

DISCUSSION

We would like to comment on the sensitivity of our technique and its applicability to measurements of the polarizability and its anisotropies in molecular systems, particularly those that absorb visible light. A typical silica microsphere ($Q \sim 10^6$) coated with biomolecules at a surface density of the order of 10^{13} cm^{-2} can resolve the polarizability change ($\Delta\alpha$) of ~3 au (~0.4 Å^3) in the near-IR. The rough estimate assumes an experimental resolution for the resonant shift of ~1/50 of the linewidth (6,7). The sensitivity is rather remarkable considering that the polarizability of a hydrogen molecule is ~0.8 Å^3, *trans-cis* isomerization of a single C-C bond and deprotonation can change the polarizability by hundreds of atomic units (24). Although conformational changes in such systems have been observed qualitatively by CPWR (14, 34) and indirectly by Stark spectroscopy (35), the magnitude of $\Delta\alpha$ that accompanies structural transformations in complex proteolipid macromolecules remains unknown. Given their superior sensitivity and the ability to directly quantify $\Delta\alpha$, the microresonators represent a new quantitative tool for probing molecular transformations in important proteolipid biomolecular assemblies such as G-protein-coupled receptors or in signaling molecules such as calmodulin and disease-related prion proteins. As shown herein for the model case of *bR*, the introduced technique is particularly suited for off-resonant pump-probe studies of photosensitive biomolecules. Further examples of such systems include photosynthetic membranes and photoreceptors such as photoactive yellow protein (36). The latter exhibits particularly large polarizability changes of ~1,000 $Å^3$ and can be therefore used as a photochromic label in fusion proteins to study molecular processes and anisotropies imposed by their e.g. proteolipid environment. Most importantly however, further improvements of the microresonator technique promise single-molecule sensitivity (22) which is beyond the scope of any alternative label-free technique.

ACKNOWLEDGEMENTS

This work was supported by the Rowland Junior Fellowship program.

REFERENCES

1. Spillane, S. M., T. J. Kippenberg, and K. J. Vahala. 2002. Ultralow-threshold Raman laser using a spherical dielectric microcavity. Nature 415:621-623.
2. Almeida, V. R., C. A. Barrios, R. R. Panepucci, and M. Lipson. 2004. All-optical control of light on a silicon chip. Nature 431:1081-1084.
3. Ilchenko, V. S., A. A. Savchenkov, A. B. Matsko, and L. Maleki. 2004. Nonlinear optics and crystalline whispering gallery mode cavities. Phys. Rev. Lett. 92:043903.
4. Krioukov, E. , D. J. W. Klunder, A. Driessen, J. Greve, and C. Otto. 2002. Sensor based on an integrated optical microcavity. Opt. Lett. 27: 512-514 (2002).
5. Armani, A. M., and K. J. Vahala. 2006. Heavy water detection using ultra-high-Q microcavities. Opt. Lett. 31:1896-1898.
6. Vollmer, F., D. Braun, A. Libchaber, M. Khoshsima, I. Teraoka, and S. Arnold. 2002. Protein detection by optical shift of a resonant microcavity. Appl. Phys. Lett. 80:4057-4059.
7. Vollmer, F., S. Arnold, D. Braun, I. Teraoka, and A. Libchaber. 2003. Multiplexed DNA quantification by spectroscopic shift of two microsphere cavities. Biophys. J. 85:1974-1979.
8. Noto, M., F. Vollmer, D. Keng, I. Teraoka, and S. Arnold. 2005. Nanolayer characterization through wavelength multiplexing of a microsphere resonator. Opt. Lett. 30:510-512.
9. Homola, J., S. S. Yee, and G. Gauglitz, 1999. Surface plasmon resonance sensors: review. Sens. Actuators B 54:3-15.

10. Lavers, C. R., K. Itoh, S. C. Wu, M. Murabayashi, I. Mauchline, G. Stewart, and T. Stout. 2000. Planar optical waveguides for sensing applications. Sens. Actuators B 69:85-95.

11. Ramsden, J. J. 1999. OWLS: A versatile technique for sensing with bioarrays. Chimia 53:67-71.

12. Salamon, Z., H. A. Macleod, and G. Tollin. 1997. Coupled plasmon-waveguide resonators: A new spectroscopic tool for probing proteolipid film structure and properties. Biophys. J. 73:2791-2797.

13. Ramsden, J. J. 1999. Molecular orientations in lipid bilayers. Philos. Mag. B 79:381-386.

14. Alves, I. D., S. M. Cowell, Z. Salamon, S. Devanathan, G. Tollin, and V. J. Hruby. 2004. Different structural states of the proteolipid membrane are produced by ligand binding to the human delta-opioid receptor as shown by plasmon-waveguide resonance spectroscopy. Mol. Pharmacol. 65:1248-1257.

15. Boxer, S. G. 1996. Stark Spectroscopy of Photosynthetic Systems. Academic Publishers, The Netherlands.

16. Birge, R. R. 1990. Photophysics and molecular electronic applications of the rhodopsins. Annu. Rev. Phys. Chem. 41:683-733.

17. Blaurock, A. E., and D. Stoeckenius. 1971. Structure of purple membrane. Nature New Biol. 233:152-154.

18. Luecke, H., B. Schobert, H.-T. Richter, J.-P. Cartailler, and J. K. Lanyi. 1999. Structural changes in bacteriorhodopsin during ion transport at 2 Angstrom resolution. Science 286:255-260.

19. He, J.-A., L. Samuelson, L. Li, J. Kumar, and S. K. Tripathy. 1999. Bacteriorhodopsin thin film assemblies - Immobilization, properties, and applications. Adv. Mater. 11:435-446.

20. He, J.-A. , L. Samuelson, L. Li, J. Kumar, and S. K. Tripathy. 1998. Oriented bacteriorhodopsin/polycation multilayers by electrostatic layer-by-layer assembly Langmuir 14:1674-1679.

21. Feringa, B. L. ed.. 2001. Molecular Switches. Wiley-VCH GmbH, Weinheim.

22. Arnold, S., M. Khoshsima, I. Teraoka, S. Holler, and F. Vollmer. 2003. Shift of whispering-gallery modes in microspheres by protein adsorption. Opt. Lett. 28:272-274.

23. Salamon, Z., and G. Tollin. 2001. Optical anisotropy in lipid bilayer membranes: Coupled plasmon-waveguide resonance measurements of molecular orientation, polarizability, and shape. Biophys. J. 80:1557-1567.

24. Toto, J.L., T.T. Toto, and C. P. de Melo. 1994. *Ab initio* studies of the polarizabilities of retinal analogs. J. Chem. Phys. 101:3945-3951.

25. Noto, M., M. Khoshsima, D. Keng, I. Teraoka, V. Kolchenko, and S. Arnold. 2005. Molecular weight dependence of a whispering gallery mode biosensor. Appl. Phys. Lett. 87:223901.

26. Porschke. D, 2003. Strong bending of purple membranes in the m-state, J. Mol. Biol. 331:667-679.

27. Sasaki, J., Y. Shichida, J. K Lanyi, J. K., and A. Maeda. 1992. Protein changes associated with reprotonation of the Schiff base in the photocycle of Asp96-->Asn bacteriorhodopsin. The MN intermediate with unprotonated Schiff base but N-like protein structure J. Biol. Chem. 267:20782 -20786.

28. Zeisel, D. and N. Hampp. 1992. Spectral relationship of light-induced refractive index and absorption changes in bacteriorhodopsin films containing wild type BR_{WT} and the variant BR_{D96N}. J. Phys. Chem. 96:7788-7792.

29. Ormos, P., L. Fábián, L. Oroszi, E. K. Wolf, J. J. Ramsden, and A. Dér. 2002. Protein-based integrated optical switching and modulation. Appl. Phys. Lett. 80:4060-4062.

30. Burland, D. M., and C. Bräuchle. 1982. The use of holography to investigate complex photochemical reactions. J. Chem. Phys. 76:4502-4512.

31. Zhang, C., Q. Wang Song, C.-Y. Ku, R. B. Gross, and R. R. Birge. 1994. Determination of the refractive index of a bacteriorhodopsin film. Opt. Lett. 19:1409-1411.

32. Thoma, R., N. Hampp, C. Bräuchle, and D. Oesterhelt. 1991. Bacteriorhodopsin films as spatial light modulators for non-linear filtering. Opt. Lett. 21:651-653.

33. Heyn, M. P., B. Borucki, and H. Otto. 2000. Chromophore reorientation during the photocycle of bacteriorhodopsin: experimental methods and functional significance. Biochimica et Biophysica Acta 1460:60-74.

34. Sota, H., Y. Hasegawa, and M. Iwakura. 1998. Detection of conformational changes in an immobilized protein using surface plasmon resonance. Anal. Chem. 70:2019-2024.

35. Bublitz, G. U., and S. G. Boxer. 1997. Stark spectroscopy: Applications in chemistry, biology, and materials science. Annu. Rev. Phys. Chem. 48:213-242.

36. Premvardhan, L. L., M. A. van der Host, K. J. Hellingwerf, and R. van Grondelle. 2003. Stark spectroscopy on photoactive yellow protein, E46Q, and a nonisomerizing derivative, probes photo-induced charge motion. Biophys. J. 84: 3226-3239.

FIGURE LEGENDS

Figure 1

(a) Experimental optical measurement set-up. P_1, P_2, polarizers; $\lambda/2$, half-waveplate; PD_1, PD_2, near-IR photodiodes; PC, personal computer for data acquisition and analysis. (b) Sample cell schematic. TE and TM-polarized WGMs in a *bR*-coated silica microsphere on a stem excited by the evanescent field coupling from a tapered optical fiber. (c) 3D ribbon-model of seven transmembrane α-helixes (green) representing the structure of *bR* protein embedded in a lipid bilayer (yellow) with a covalently bound all-*trans* retinal chromophore (red). Linearly polarized microcavity resonances probe the protein in the direction orthogonal to (TM) or parallel with (TE) the *bR* membrane adsorbed on the microsphere surface (xy-plane).

Figure 2

The time trace of a TM-polarized resonance wavelength shifts due to *bR* adsorption from a liquid solution that surrounds the microcavity. The measured resonant shift at saturation, $\Delta\lambda \cong 67$pm, points to self-assembly of a *bR* monolayer.

Figure 3

Dynamics of the ground to M state transformation observed by tracking wavelength shifts of TE- and TM-polarized microcavity modes.

Figure 4

Transmission spectra for a TE and a TM polarized WGM. A negative resonance wavelength shift is observed upon photoexcitation of the adsorbed *bR* monolayer. The shift is about twice as large for the TE than for the TM mode, which is due to the retinal orientation in the *bR* membrane.

Figure 5

Angles defining the average orientation of the retinal relative to the polarization direction of the probing resonances.

Topolancik&Vollmer_Figure 1

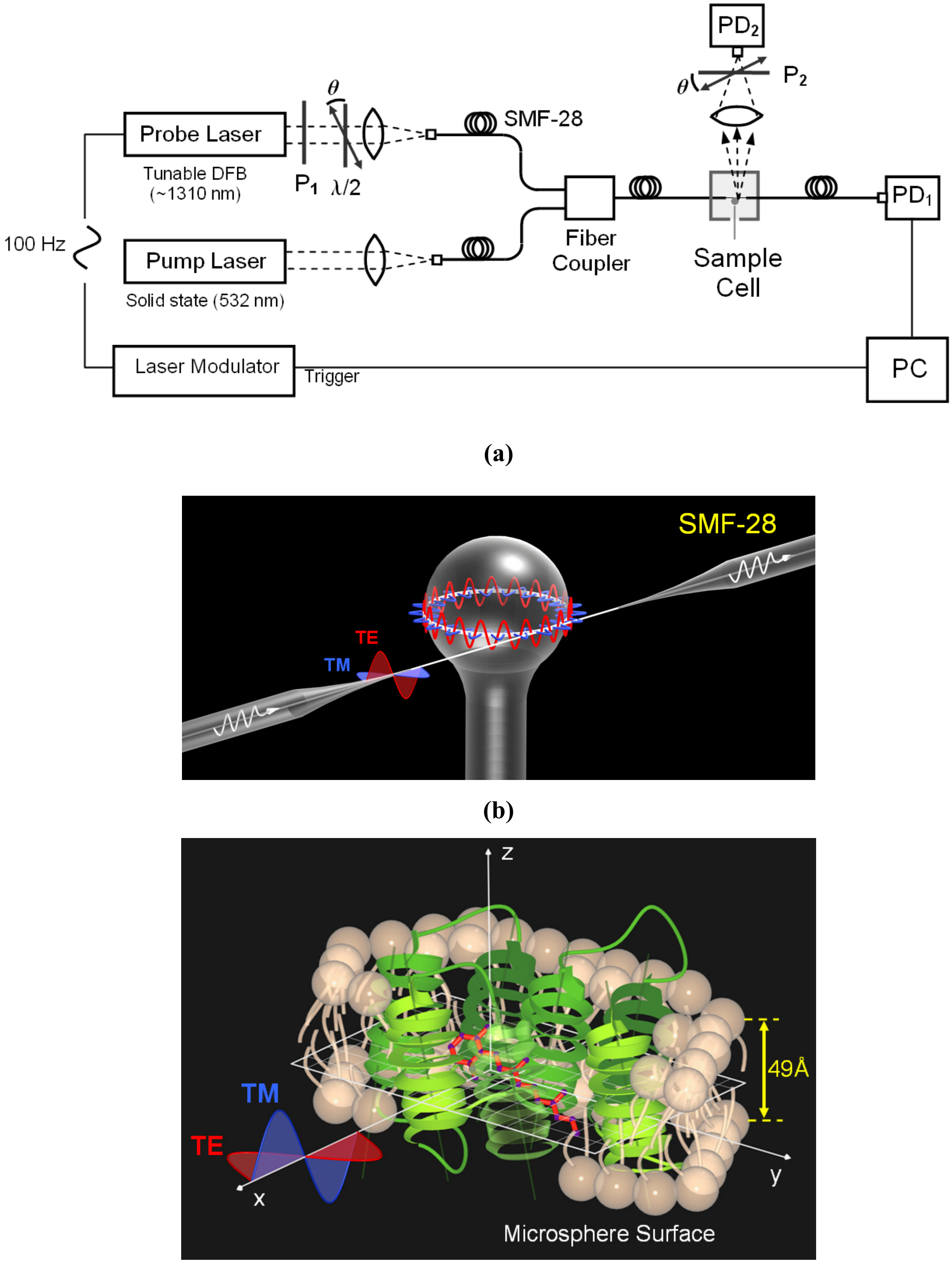
PD$_2$
P$_2$
θ
θ
Probe Laser
Tunable DFB
(~1310 nm)
P$_1$
λ/2
SMF-28
Fiber
Coupler
Sample
Cell
PD$_1$
100 Hz
Pump Laser
Solid state (532 nm)
Laser Modulator
Trigger
PC
SMF-28
TE
TM
z
49Å
TM
TE
x
y
Microsphere Surface

(a)

(b)

(c)

Topolancik&Vollmer_Figure 2

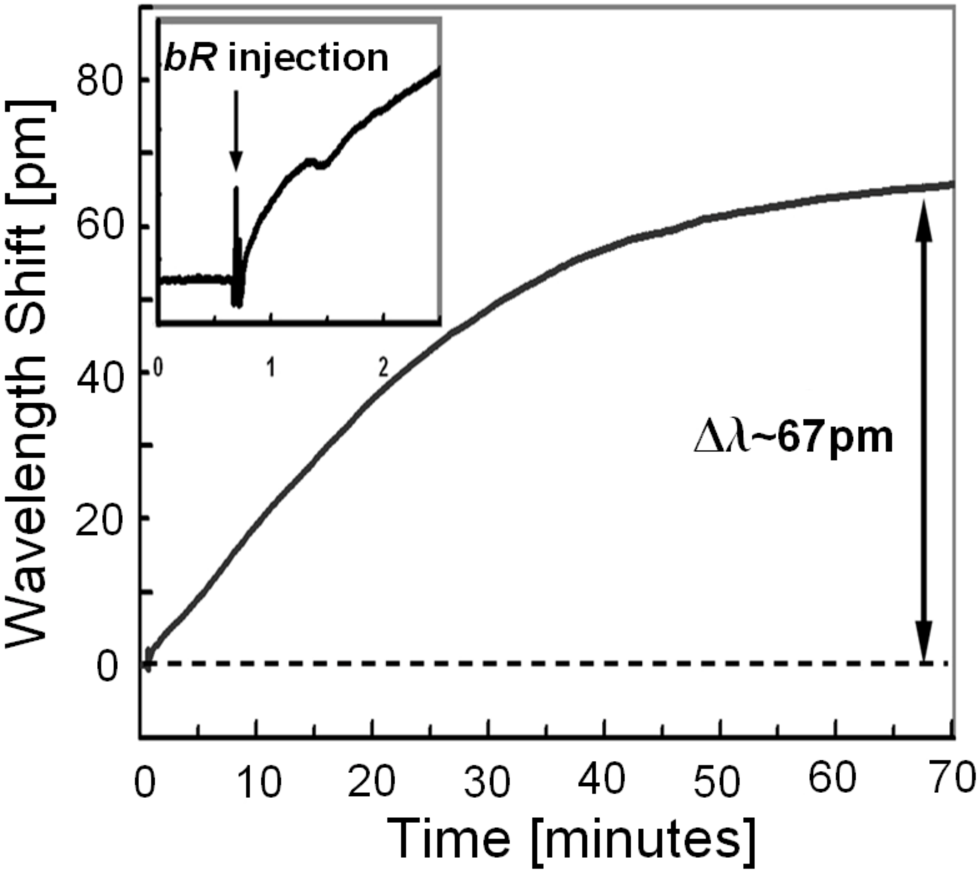

Topolancik&Vollmer_Figure 3

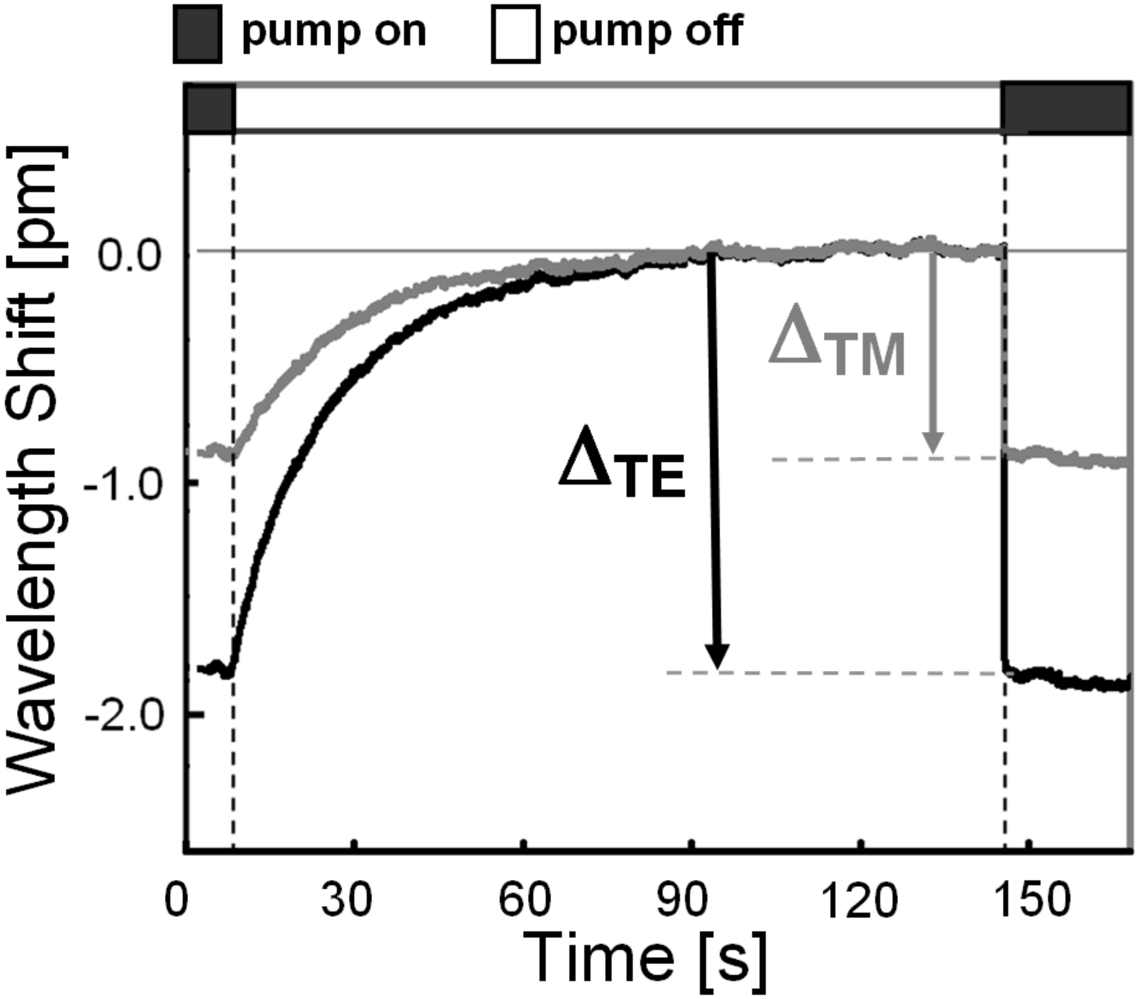

Topolancik&Vollmer_Figure 4

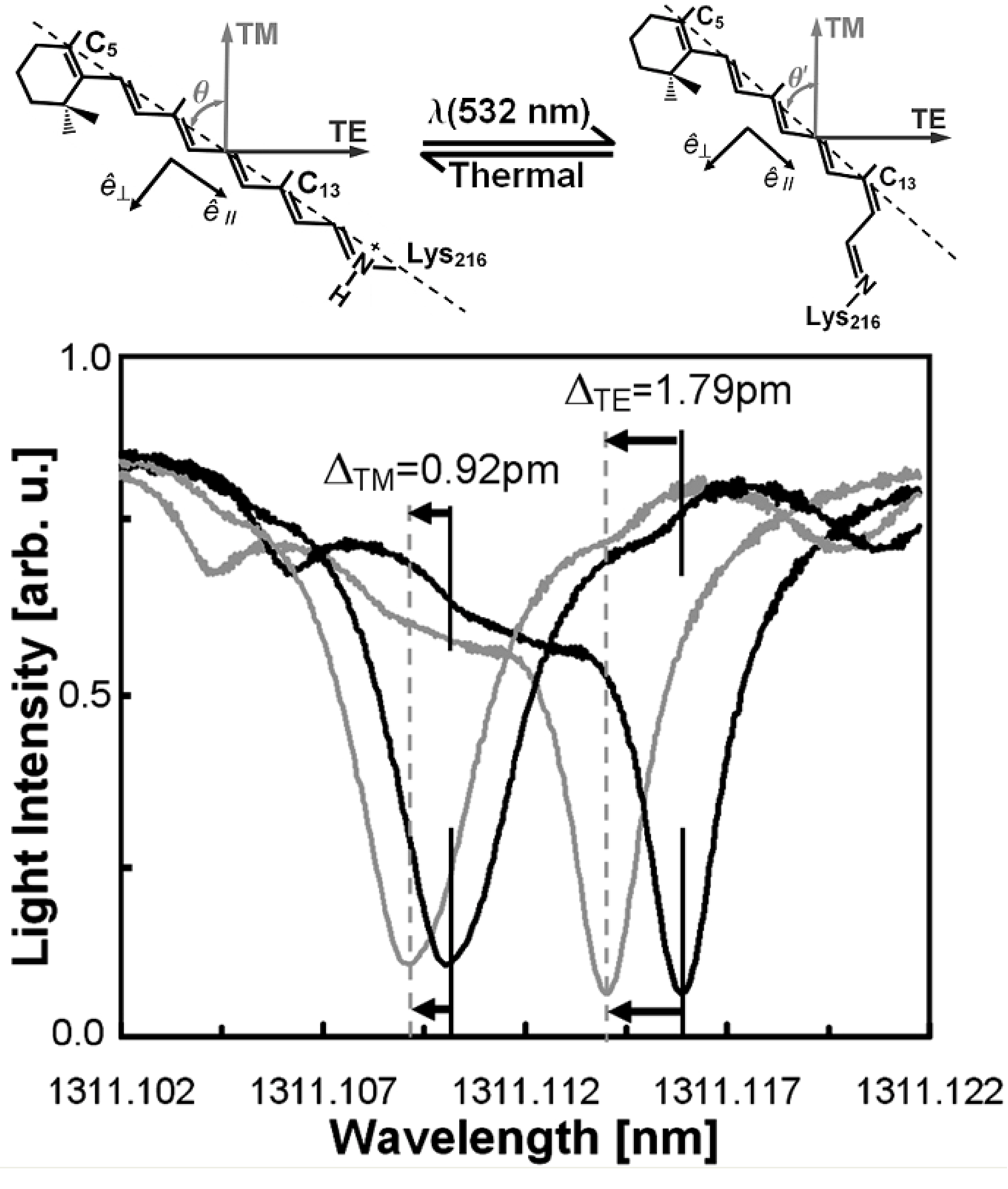

Topolancik&Vollmer_figure 5

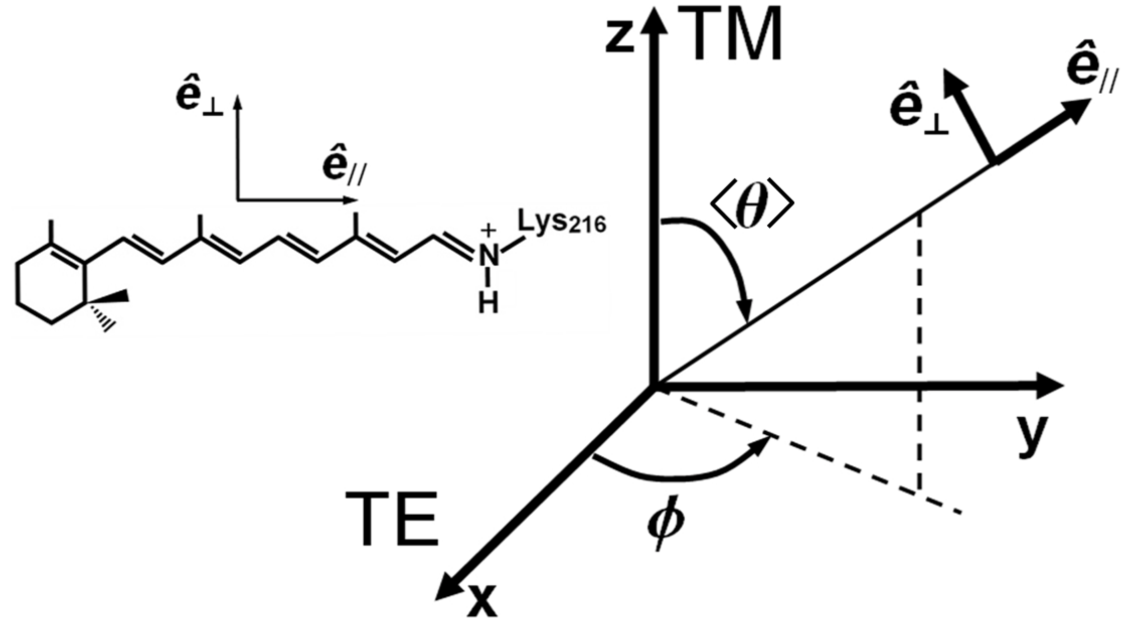
ê⊥
ê//
+
N
H
Lys216
z
TM
ê⊥
ê//
⟨θ⟩
y
TE
φ
x